frontiers | Frontiers in Earth Science

TYPE Original Research
PUBLISHED 18 January 2024
DOI 10.3389/feart.2023.1303330

Check for updates

OPEN ACCESS

EDITED BY
Carmen Solana,
University of Portsmouth, United Kingdom

REVIEWED BY
James Martin Dines Day,
University of California, San Diego,
United States
Chiara Scaini,
National Institute of Oceanography and Applied Geophysics, Italy

*CORRESPONDENCE
María-Paz Reyes-Hardy,
maria-paz.reyeshardy@unige.ch

RECEIVED 27 September 2023
ACCEPTED 29 December 2023
PUBLISHED 18 January 2024

CITATION
Reyes-Hardy M-P, Biass S, Dominguez L, Di Maio LS, Frischknecht C, Bonadonna C and Pérez N (2024), Temporal evolution of roof collapse from tephra fallout during the 2021-Tajogaite eruption (La Palma, Spain). *Front. Earth Sci.* 11:1303330. doi: 10.3389/feart.2023.1303330

COPYRIGHT
© 2024 Reyes-Hardy, Biass, Dominguez, Di Maio, Frischknecht, Bonadonna and Pérez. This is an open-access article distributed under the terms of the Creative Commons Attribution License (CC BY). The use, distribution or reproduction in other forums is permitted, provided the original author(s) and the copyright owner(s) are credited and that the original publication in this journal is cited, in accordance with accepted academic practice. No use, distribution or reproduction is permitted which does not comply with these terms.

Temporal evolution of roof collapse from tephra fallout during the 2021-Tajogaite eruption (La Palma, Spain)

María-Paz Reyes-Hardy[1]*, Sébastien Biass[1], Lucia Dominguez[1], Luigia Sara Di Maio[1], Corine Frischknecht[1], Costanza Bonadonna[1] and Nemesio Pérez[2,3]

[1]Department of Earth Sciences, University of Geneva, Geneva, Switzerland, [2]Instituto Tecnológico y de Energías Renovables (ITER), Tenerife, Canary Islands, Spain, [3]Instituto Volcanológico de Canarias (INVOLCAN), Tenerife, Canary Islands, Spain

Although dominantly effusive, the 2021 Tajogaite eruption from Cumbre Vieja volcano (La Palma, Spain) produced a wide tephra blanket over 85 days of activity. About one month after the eruption onset, clean-up operations were implemented to mitigate the impact of tephra load on primary buildings. Here, we present a post-event impact assessment of 764 primary buildings, which expands our empirical knowledge of building vulnerability to tephra fallout to include impacts from long-lasting eruptions. Field observations are analyzed in the perspective of existing fragility curves, high-resolution satellite imagery and a reconstruction of the spatio-temporal evolution of the tephra blanket to characterize the evolution of roof collapse due to static loads over time. Thanks to a chronological correlation between the temporal evolution of tephra sedimentation and the timing of clean-up operations, we quantified their effectiveness in mitigating roof collapse. If no clean-up measures had been taken 11% of the surveyed buildings would have exceeded a 75% probability of roof collapse, while only 10 roof collapses have been observed (1.3% of the analysed buildings). This work provides key insights for further development of emergency plans for the management of long-lasting eruptions characterised by the sustained emission of tephra over weeks to months.

KEYWORDS

Cumbre Vieja volcano, tephra impact, vulnerability roof classes, building roof collapse, tephra clean-up, fragility curves

1 Introduction

The 2021 Tajogaite eruption of Cumbre Vieja volcano (La Palma, Spain) has demonstrated the complexity of managing long-lasting volcanic crises characterised by the concurrence of hazard related to both effusive and explosive styles. The management of such crises, with durations varying from a few weeks to a few years, is typically associated with large uncertainties in relation to the spatio-temporal evolution of the associated hazards. Here, *hybrid eruption* refer to the simultaneous emission of lava flows and tephra (Pioli et al., 2009; Bonadonna et al., 2022; Wadsworth et al., 2022), causing multiple hazards able to interact and evolve into compound impacts that further increase uncertainty that

authorities must handle during decision-making processes. Preventive evacuation of the most exposed areas is usually the first mitigation strategy adopted in volcanic crises (e.g., 2007 Kelut (De Bélizal et al., 2012), 2010 Merapi (Mei et al., 2013), 2010 Sinabung and 2014 Kelut eruptions, Indonesia (Andreastuti et al., 2019)) and is an effective way to minimize fatalities or injuries (Lindell and Perry, 1993; UNISDR, 2009; Marrero et al., 2013; Tomsen et al., 2014). However, evacuation is only one of the various measures that can be taken to reduce risk. Other actions such as clean-up operations of tephra fallout can also be adopted to mitigate impacts on residential buildings, infrastructure, and lifelines if informed emergency plans are in place (e.g., Wilson et al., 2007; 2013; Blake et al., 2015; Biass et al., 2016; Hayes et al., 2019).

The 2021 Tajogaite eruption, which lasted for 85 days and was characterized by the simultaneous emission of tephra, lava, and gas as well as multiple shifts in eruptive vents and styles (e.g., Hawaiian, Strombolian, violent Strombolian, lava fountaining, ash-poor gas puffing; Bonadonna et al., 2023; Taddeucci et al., 2023), provides a recent example of challenges associated with the management of such volcanic crisis (Longpré, 2021; Carracedo et al., 2022). It impacted human settlements with a cost of 842 M€ (165 M€ estimated for total destruction of houses) and forced the evacuation of more than 7,000 residents (Comisión mixta para la reconstrucción and recuperación y apoyo a la isla de La Palma, 2022). In total, 10 out of 14 municipalities of the island were directly and indirectly affected by a significant disruption on the transportation network and, overall, the Department of Geological Risks and Climate Change of the Geological and Mining Institute of Spain (IGME-CSIC) estimates that a total of about 20,000 people were exposed to the eruption and its consequences (López et al., 2021). More specifically, nearly 1,300 ha of land was affected and covered by lava flows, of which three municipalities were directly affected with nearly 3,000 houses destroyed (Comisión mixta para la reconstrucción and recuperación y apoyo a la isla de La Palma, 2022), 74 km roads, and 3.7 km^2 of crops (i.e., 2.3 km^2 banana tree, 0.7 km^2 vineyard, and 0.3 km^2 avocado) were buried by lava flows (https://volcan.lapalma.es/), while the entire island was affected by tephra [i.e., including bombs in proximal area, and lapilli, and ash in medial and distal areas, respectively; Day et al. (2022a)]. Tephra was mostly dispersed NE-SW due to a complex regional and local wind pattern (Bonadonna et al., 2022). Coarse ash to lapilli significantly impacted the SW of the island (e.g., streets, public infrastructure, commercial and residential buildings), while fine ash was also recorded on the neighboring islands, such as Tenerife, El Hierro and even Gran Canaria (López et al., 2021), causing 21 days of closure of La Palma airport in addition to 8 days of disruption (Rey et al., 2023), including the cancellation of more than 300 flights (Longpré, 2021).

Tephra loads on buildings can cause structural damage and subsequent roof collapses (Blong, 1984; Jenkins et al., 2015). The intensity of the resulting impact not only depends on the physical characteristics of tephra deposits (e.g., load), but also on the specific vulnerability of the built environment (Jenkins et al., 2017; Bonadonna et al., 2021). The crisis management strategy adopted during the 2021 Tajogaite eruption included such actions as tephra clean-up operations that resulted in a limited number of collapsed roofs (Rey et al., 2023). In this context, accurate vulnerability models contribute to better inform the development of mitigation measures in emergency response and, ultimately to reduce the potential impacts (Jenkins et al., 2015). Efforts at compiling models describing the physical vulnerability of buildings dominantly rely on post-event impact surveys attempting to constrain a relationship between hazard intensity and a degree of impact, and have taken various shapes (e.g., damage/disruption scales, vulnerability and fragility functions; Wilson et al., 2011; Wilson et al., 2014a; Jenkins et al., 2015; Wilson et al., 2017). Amongst existing literature on impacts to the built environment only two studies present an impact assessment on a significant numbers of buildings (i.e., Spence et al., 1996; Blong, 2003). Based on these studies and complementing them with theoretical calculations and experiments, Spence et al. (2005) developed generic fragility curves expressing the probability of occurrence of one damage state (here, roof collapse) under a static tephra load for the European built environment (Spence et al., 2005; Wilson et al., 2014a). Although these fragility curves were further refined for specific case-studies (e.g., Naples, Italy; Zuccaro et al. (2008); around Kanlaon, Philippines and Fogo, Cape Verde Volcanoes; Jenkins et al. (2014)), the generic fragility curves of Spence et al. (2005) allow a first order assessment of the potential damage of future eruptions where dedicated vulnerability studies lack (Douglas, 2007).

Here, we present a post-event impact assessment of the tephra fallout on buildings following the 2021 Tajogaite eruption. By complementing field observations with existing vulnerability models, satellite imagery and discussion with local stakeholders, we quantify the extent and severity of impacts and investigate the effectiveness of clean-up operations in reducing the number of roof collapses. This study contributes to the empirical understanding of the physical vulnerability of building to tephra fallout and expands it to consider the temporal evolution of hazard metrics over ~3 months of eruption.

2 Case study

Located in front of west Africa, La Palma is one of the youngest islands (~3.0 Ma) of the Canarian Archipelago, Spain (Ancochea et al., 1994; White and Schmincke, 1999; Carracedo and Troll, 2016) (Figures 1A–D). It has two main edifices: Caldera de Taburiente to the north, a circular shield volcano formed by three large overlapping volcanoes and the Cumbre Vieja rift, a southern elongated N-S ridge structure (see Carracedo et al. (1999a; b); Carracedo and Troll (2016) for further details of the overall geology of La Palma). Several cinder cones and craters along Cumbre Vieja axis formed during the past 7,000 years indicate continuous migration of emerged volcanism from the Caldera de Taburiente towards the south (Carracedo et al., 2001; Walter and Troll, 2003; Carracedo and Troll, 2016). Historical activity in the Cumbre Vieja ridge has typically produced simultaneous explosive-effusive eruptions characterized by cinder cones, tephra deposits, and lava flow fields (Martín-Lorenzo et al., 2022). With the highest-altitude vents predominantly explosive and the lowest-altitude more effusive, the preferential lava inundation paths have often formed extensive coastal platforms (Carracedo and Troll, 2016). At least six out of the fourteen Holocene eruptive periods that the Global Volcanism Program recognizes for La Palma (GVP, 2023) reached the sea in 1585 (Hernandez-Pacheco and Valls, 1982; Hernández-Pacheco, 1990),

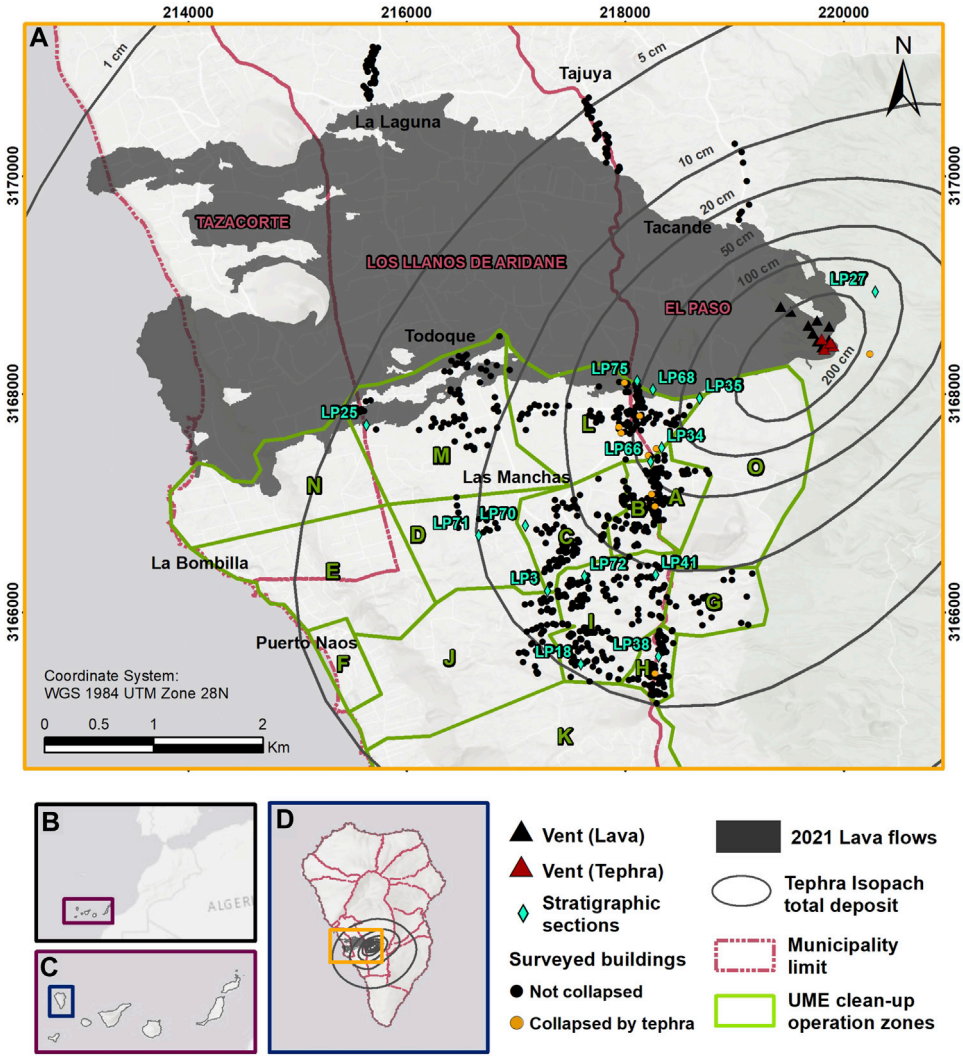

FIGURE 1
(A) Map showing our study area including the 2021 lava flows (from Copernicus EMSR546), the isopach maps of the total tephra deposit (in cm) and the reference stratigraphic sections used in this study [both from Bonadonna et al. (2022)], the Unidad Militar de Emergencias (UME) clean-up operation zones used as surveyed zones and our surveyed buildings. **(B)** Inset of the Canary Islands highlighted in a purple rectangle, **(C)** La Palma Island highlighted in a blue box, **(D)** municipality divisions of La Palma Island and location of our study area highlighted in a yellow rectangle.

1646, 1712 (Santiago, 1960; Carracedo et al., 2001), 1949 (Romero Ortiz, 1951; San Miguel de la Cámara et al., 1952; Romero and del Carmen, 1990; Klügel et al., 1999), 1971 (Praegel, 1986; Carracedo et al., 2001) and recently in 2021 (Carracedo et al., 2022).

2.1 Timeline of the 2021 eruption

After a repose period of 50 years, a new volcanic episode started on the 19 September at 15:11 UTC on the western flank of the Cumbre Vieja ridge, which lasted for 85 days until 13 December 2021. This eruption was characterized by the simultaneous emission of lava flows and tephra plumes along a ~0.5 km-long fissure that focalized on about ten vents that built a composite cinder cone (Bonadonna et al., 2022; Civico et al., 2022; Romero et al., 2022). Tephra was sedimented on most of La Palma and sporadically reached the neighboring islands, following a NE-SW direction due to the prevailing winds (Bonadonna et al., 2022). The overall volume (tephra blanket, tephra cone and subaerial lava flow) was estimated at 1–3 × 10^8 m^3, with the tephra blanket constituting <20% of the total erupted volume (2.3 × 10^7 m^3; Bonadonna et al., 2022). In terms of surface, lava flows covered an area of 12.4 km^2 out of the total 87.9 km^2 impacted by the overall eruption (Lev et al., 2022). The highest observed plume reached an elevation of 8,500 m a.s.l. and occurred some hours before the end of the eruption, whilst the average plume height was ~3,500 m a.s.l. (Felpeto et al., 2022). Tephra grainsize distributions on land were dominated by lapilli and coarse ash with an overall high vesicularity, mafic composition (i.e., basanite–alkali basalt), and bulk densities varying between 634 and 1491 kg/m^3 (Bonadonna et al., 2022; 2023).

During the first days of the eruption, estimated SO_2 emission rates reached more than 30,000 tons day^{-1}, maintaining weekly average values above 10,000 tons day^{-1} until the end of the eruption (Albertos et al., 2022; Hayer et al., 2022). After a final

TABLE 1 Preliminary aspects identified remotely for the vulnerability classification of roofs.

Roof configuration	Roof covering material	Roof regularity/design
S: Single pitch	C: Concrete	0: Regular plan/simple design
A: Two or more pitches	T: Tiles	1: Regular plan/composite design
F: Flat	M: Metallic	2: Irregular plan/composite design
--	X: Fiber cement, zinc, plastic	--

paroxysmal phase on 12–13 December 2021, the estimated SO_2 emission rates decreased significantly to ~250 tons day^{-1} (Albertos et al., 2022). However, significant gas emissions in the areas of Puerto Naos and La Bombilla remain active until at least the 7th July 2023 (PEVOLCA, 2023).

3 Materials and methods

To quantify the extent and severity of tephra fallout impacts on roofs and the effectiveness of clean-up operations, we designed a post-eruption impact assessment based on the protocol of Dominguez et al. (2021). This methodology includes 4 steps that are i) defining the objectives and level of detail of this study; ii) exploring evidences of impact caused by tephra on the built-environment; iii) quantifying impacts based on observations of damage and buildings properties in relation with tephra thickness; and iv) identifying critical aspects that played a major role on reducing impacts (e.g., response actions). Prior to the first visit, we defined survey zones considering the prevailing direction of tephra sedimentation and the UME (Unidad Militar de Emergencias) tephra clean-up operation zones (Figure 1) to perform a preliminary classification of buildings based on roof typologies using high-resolution satellite imagery available on Google Earth. Three field campaigns (on 21 October—05 November 2021; 07–18 February 2022; and 14–20 May 2022) were conducted to document the occurrence of roof collapse of primary buildings (i.e., closed constructions that have the functions of housing, services, or commercial use). Secondary buildings (i.e., small independent constructions with a minor function such as warehouses, rural and farm buildings, water tanks, garages, and outdoor kitchens) and annexes (i.e., structurally dependent constructions and parts of primary and secondary buildings such as storages, verandas, huts, and sheds) are not included in this survey. The tephra load for all primary surveyed buildings was reconstructed using the isopach maps of Bonadonna et al. (2022). Clean-up operations were reconstructed based on information provided by the UME agents. All survey information was stored in a geographic information system (GIS).

3.1 Characterization of the built environment

We focus here on the roof collapse damage state and use the European tephra fallout roof fragility curves developed by Spence et al. (2005) as a basis for our study. Pre-eruption satellite imagery of La Palma Island was used for a preliminary assessment of roof typologies of the buildings located in our survey zones. Based on the morphology and surface appearance of the roofs, roof typologies were identified considering three main aspects (e.g., configuration, covering materials, and regularity in plan/design) using a specific code (Table 1). By configuration we refer to the steepness or angle at which a building roof surface deviates from the horizontal, easily recognizable from aerial, oblique or street view (when possible), looking at the different planes and ridges of the roof covering. Most covering materials were recognized by looking for patterns, shapes, colors, and textures such as red to reddish orange for most clay tiles, rough gray surfaces for flat surface in concrete (e.g., concrete or reinforced concrete slab), sometimes with red or green paint finishes, and smooth textured surfaces in the form of wavy folds or alternating grooves and ridges with bright gray, reddish or greenish colors for metallic sheets. Following the European Design of structures for earthquakes resistance code (EN, 1998-1, 2004), the regularity in plan is for building structures that have a compact and symmetrical configuration. We included simple and composite design in this description, to describe roof coverings of only one type of material or more than two respectively.

3.1.1 Syn- and post-eruption impact assessment

Roof collapse considers failure of the roof covering and/or of the supporting structures (Spence et al., 2005; Jenkins et al., 2014); we therefore investigated such parameters such as roof covering material and supports, shape and pitch. Three field campaigns were conducted in the areas most exposed to tephra fallout during and after the Tajogaite eruption (Figure 2A shows the landscape before the eruption onset for comparison). During the first field campaign (21 October—5 November 2021, Figure 2B), when limited access to structures was possible, we validated the remote classification of roof typologies and developed a first-order classification of the building typologies. Additionally, we included typological aspects such as type of vertical structure (e.g., regular and irregular masonry structures, wooden, mixed structures or reinforced concrete structures), number of storeys (e.g., single-storey, two or more storeys), coordinates, photos and notes about the roof collapses. For example, regular masonry was recognized as constituted by regular shape elements, such as cement bricks and concrete blocks. Irregular masonry structures on the reverse, as constructions constituted by elements without any regular shape or elements of different size with sharp edges, such as rough or broken stones, used as the basic building material. We elaborated a standardized form (see Supplementary Figure S1), based on other studies (e.g., Grünthal, 1998; Spence et al., 2005;

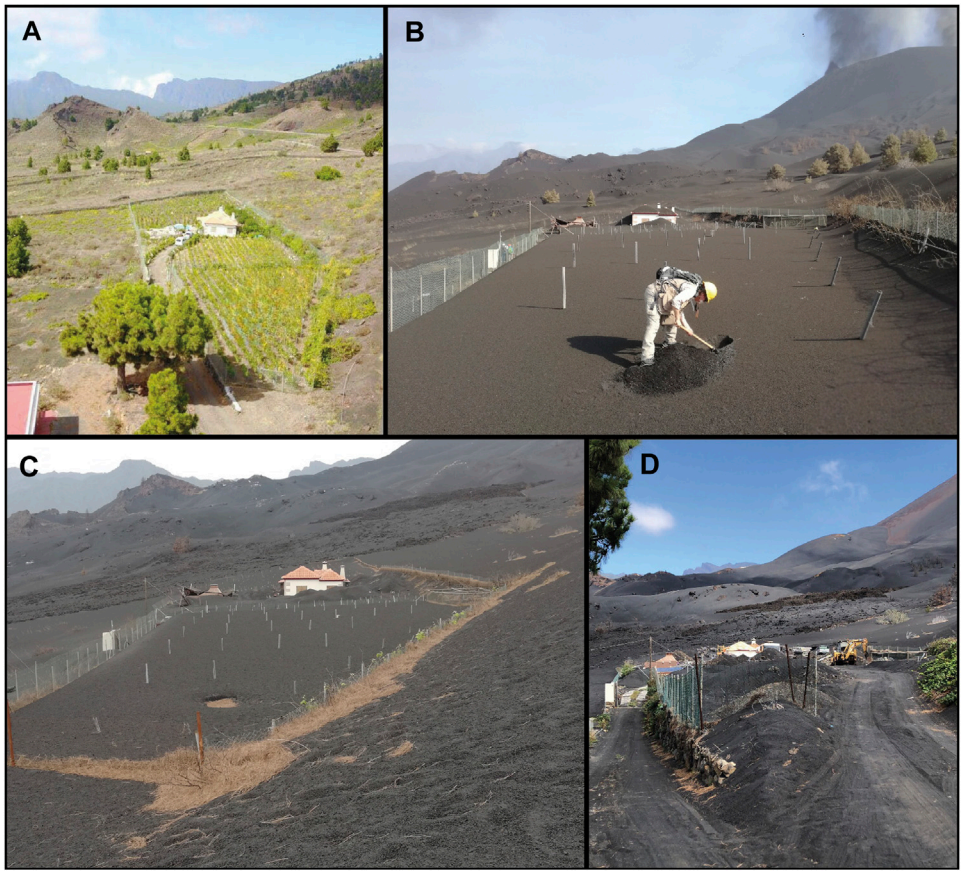

FIGURE 2
Evolution of the state of a property located about 1 km SW from the Tajogaite cone: **(A)** before the eruption (Photo: courtesy of Julio Rodriguez Diaz and Pedro Garcia Salguero), **(B)** during the eruption (29 October 2021), **(C)** 2 months after the eruption (9 February 2021), and **(D)** almost a year after the eruption (September 2022, photo: courtesy of Marco Pistolesi). All pictures are approximately oriented towards NNW.

Baggio et al., 2007; Jenkins et al., 2014). Using this form, a group of two to four people surveyed 300 buildings.

Once the eruption stopped, we further surveyed 464 buildings following the same approach during two extra field campaigns (7–18 February 2022 (Figure 2C) and 14–20 May 2022). In total, 764 out of 6,057 buildings were surveyed in 10 out of the 15 UME clean-up operation zones [i.e., A = 57/229, B = 62/545, C = 91/1056, D = 18/174, G = 25/76, H = 82/351, I = 115/1092, J = 78/456, L = 104/954, and M = 61/1124, the estimated number of primary buildings per area are extracted from Ministerio de Hacienda y Función Pública (2014)] which were considered to be representative of the diversity of vulnerability roof classes of the area (see Figure 1 for location of UME zones and surveyed buildings). Additionally, zone TTLL (Tacande, Tajuya and La Laguna neighborhoods) was added to group the surveyed buildings outside of the UME clean-up operation zones in the north of lava flows, in addition with the isolated building at the East of the vent (a total of 71 buildings, Figure 1). Finally, the physical characteristics of our surveyed buildings were compared with previous vulnerability classes descriptions (i.e., Spence et al., 2005; Marti et al., 2008) and assigned a vulnerability class to each roof typology, including weak (WE), medium weak (MW), medium strong (MS), and strong (ST) (Table 2). Figure 2D shows the landscape after a year of the eruption onset for comparison.

3.2 Spatio-temporal evolution of the tephra blanket

The spatio-temporal evolution of the tephra blanket was reconstructed using the isopach maps of Bonadonna et al. (2022). Temporal constraints were inferred for all units and sub-units by comparing stratigraphic logs with syn-eruptive pictures and geophysical monitoring (Bonadonna et al., 2022). All interpolations were performed in *Python v3.9*. Isopach maps were interpolated in space on a 100x100 m grid using *Radial Basis Functions* in *Scipy v1.9* (Gommers et al., 2022). Each grid was then loaded in *xarray v0.21.0* (Hoyer et al., 2022) and linearly interpolated in time. Tephra thickness was converted into a mass accumulation per unit area using a mean bulk deposit density of 1,200 kg/m^3 inferred from the average density of all layers (Bonadonna et al., 2022), and to a load using:

$$I = \rho g h / 1000 \quad (1)$$

Where I is the hazard intensity (tephra load (kPa)), g =gravitational acceleration (9.80665 m/s^2), h = tephra thickness or depth (m), ρ = tephra deposit density (kg/m^3). A comparison between interpolated values and observed tephra loads is presented in Supplementary Figure S2.

Following Biass et al. (2016), interpolated tephra loads were converted into probabilities of roof collapse using the fragility curves of Spence et al. (2005):

TABLE 2 Comparison of observed building properties with roof classes of Spence et al. (2005) and Marti et al. (2008). The typical design loads and mean estimated collapse loads from these previous works are also included.

Roof classes	Description			Typical design load range	Mean collapse load (kPa)
	Our survey	Spence et al. (2005)	Marti et al. (2008)		
WE (weak)	- Roofs made of metallic, fiber cement, zinc, or plastic sheets, regular plan and simple design or irregular plan/composite design of all kinds of angles and masonry (i.e., S-A-F/X/0–2/R-I-B). - Tiled roofs with two or more pitches, regular plan and simple design or irregular plan/composite designand wooden masonry (i.e., A/T/0–2/W).	- Sheet roofs (i.e., X), old or in poor condition. - Tiled roof (i.e., T), old or in poor condition. - Masonry vaulted roof.	Old pitched tile or sheet metal (i.e., T or X).	Pre-design or no design code	2.0
MW (medium weak)	- Tiled roof with all kinds of angles, visibly in good condition, regular plan and simple design or irregular plan/composite design, and irregular bearing masonry (i.e., S-A-F/T/0–2/I).	- Sheet roof on timber; average quality; average or good quality tiled roof on timber rafters or trusses (i.e., S-A-F/X-T). - Steel or precast reinforced concrete joists and flat terrace roof (i.e., F/C).	Modern pitched tile or sheet metal (i.e., S-A/X-T), old flat or pitched concrete (i.e., S-A-F/C).	1.0–2.0 kPa	3.0
MS (medium strong)	- Tiled roof with two or more pitches. - Tiled single pitch roof with infill in concrete blocks visibly in good condition, regular plan and simple design or irregular plan/composite design and reinforced concrete and/or masonry structure with regular or combined bearing masonry and/or infill walls (i.e., S-A/T/0–2/R-B).	- Flat reinforced concrete roof not all above characteristics; sloping reinforced concrete roof (i.e., S-F/C). - Sheet roof on timber rafters or trusses, good quality and condition, designed for cyclone areas (i.e., X).	Recent pitched tile or sheet roofs (i.e., S-A/X-T), modern flat or pitched concrete (i.e., S-F/C).	2.0–3.0 kPa	4.5
ST (strong)	- Flat roof in concrete (either concrete slab and/or reinforced concrete), of all kinds of structure regularity/design and reinforced concrete and/or masonry structure with regular, irregular, or combined bearing masonry and/or infill walls (i.e., F/C/0-1–2/R-I-B).	- Flat reinforced concrete roof designed for access; recent, good quality construction, younger than 20 years (i.e., F/C).	Recent flat or pitched concrete (i.e., S-F/C).	>3.0 kPa	7.0

$$P\left(collapse\middle|I\right) = \varphi\left(ln\left(I\right),\ ln\left(Qmean\right),\sigma\right) \quad (2)$$

Where $P\left(collapse\right)$ is the probability of roof collapse of the exposed building, $Qmean$ is the mean collapse tephra load, specific to each roof type (kPa; Table 2), σ is the geometric standard deviation fixed to 0.2 following Spence et al. (2005), and φ is the cumulative density function of a Normal distribution (Spence et al., 2005; Jenkins et al., 2014; Biass et al., 2016).

3.3 Clean-up operations

UME agents provided key insights into tephra clean-up operations undertaken during crisis response, in particular the timing of clean-up operations of roofs for each zone (Supplementary Table S1). Clean-up operations by UME started on October 12, while tephra was still falling, when the potential impacts of tephra load became obvious to authorities and building owners. However, systematic records of clean-up operations per zone began only on October 22 (see Supplementary Table S1), with an average of 20 roofs per day during the first days. Clean-up operations were initially focused on the removal of tephra on primary buildings and other structural elements to prevent collapse and were later expanded to prevent non-structural damage on critical public buildings such as schools and health centers. Operators manually removed tephra from the roofs as well as tephra accumulated against the walls to prevent horizontal overpressure and, using heavy machinery, from the road networks to preserve mobility. Street drains were also cleaned to prevent flooding caused by clogging of the drainage and sewage networks, especially in the municipalities of El Paso, Los Llanos de Aridane, and Tazacorte. On average, clean-up operations in the southern sector of the lava flow mobilized 50 people in teams of five (e.g., from the UME, municipalities and owners), with each team able to clean three to four roofs per day in optimal conditions. However, working conditions were often complicated during the eruption due to high levels of volcanic gas concentrations, bad air quality, episodes of tephra fallout, lack of light and/or adverse weather, which frequently interrupted this clean-up rate forcing the teams to leave and preventing work in those areas for entire days.

FIGURE 3
Roof and building types identified in our survey. Examples of Weak, WE **(A–C)**; Medium Weak, MW **(D–F)**; Medium Strong, MS **(G–I)**; and Strong, ST **(J–L)** classes are displayed.

We accounted for tephra clean-up operations in the temporal evolution of the tephra load (Eq. 1) on roofs by removing 100% of the tephra load on all buildings of a given zone every time the data obtained from UME indicated clean-up and recomputing the associated collapse probabilities (Eq. 2). This strategy implies two assumptions. Firstly, we assume that all roofs within a zone are cleaned when clean-up operations took place, which probably overestimates clean-up effectiveness. Secondly, we assume that no clean-up occurred before October 15. However, the visual analysis of unmanned aerial vehicles (UAV) by the Cabildo Insular of La Palma reveals that some clean-up operations might have occurred earlier in October, at least in zone L (Figure 1). Since it is impossible to constrain the timing of clean-up operations by other entities than UME, we only account for clean-up operations provided in the Supplementary Table S1 and recognize that any observed collapse probably occurred at lower load thresholds than those inferred from our reconstruction of the evolution of the tephra deposit.

4 Results

4.1 Vulnerability roof class distribution

Based on the 764 primary buildings surveyed, we defined four roof types (Figure 3):

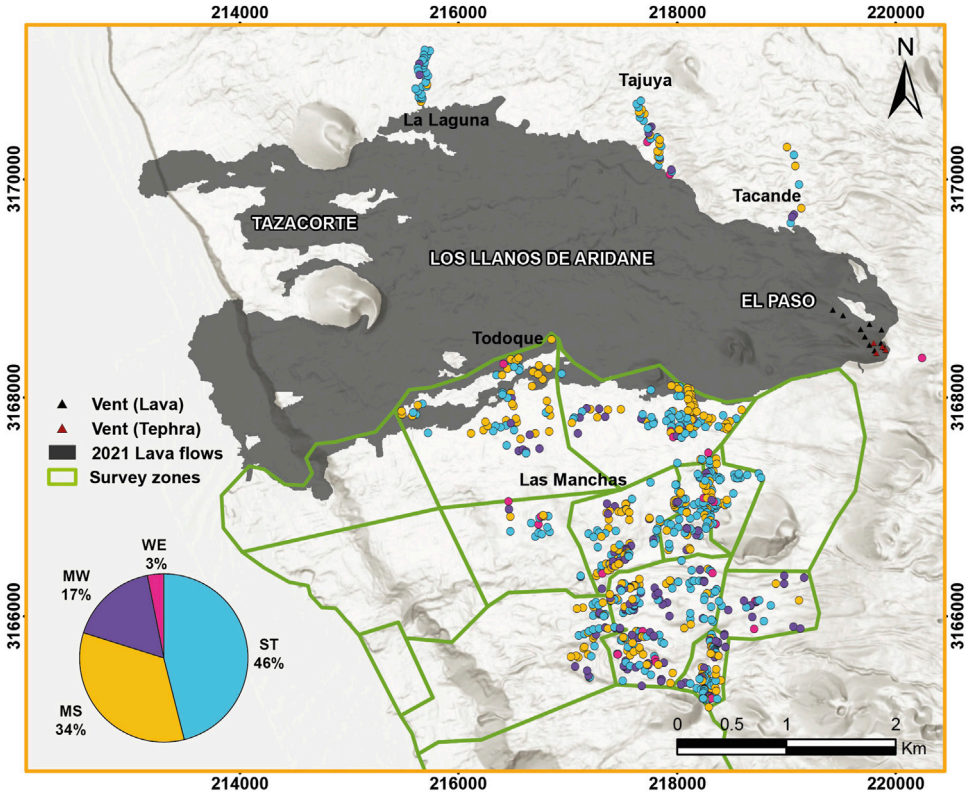

FIGURE 4
Spatial distribution (map) and percentage (pie chart) of vulnerability roof classes in the study area (WE, Weak; MW, Medium Weak; MS, Medium Strong; ST, Strong).

- Type 1: Roofs with two or more pitches, single pitch, or flat angles made of metallic, fiber cement, zinc, or plastic sheets, regular plan and simple design or irregular plan/composite design, and regular (i.e., cement bricks), irregular (i.e., broken stone), or combined bearing masonry. Tiled roofs with two or more pitches, regular plan and simple design or irregular plan/composite design and wooden masonry.
- Type 2: Tiled two or more pitches, single pitch, or flat roof (old or new) visibly in good condition, regular plan and simple design or irregular plan/composite design, and irregular bearing masonry.
- Type 3: Tiled two or more pitches and single pitched roof with infill in concrete blocks visibly in good condition, regular plan and simple design or irregular plan/composite design and reinforced concrete and/or masonry structure with regular or combined bearing masonry and/or infill walls.
- Type 4: Flat roofs in concrete (either concrete and/or reinforced concrete slab), regular plan and simple design or irregular plan/composite design, flat/composite design and reinforced concrete and/or masonry structure with regular, irregular, or combined bearing masonry and/or infill walls.

Based on the descriptions of the built environment (Table 2), we assigned a weak class (WE) to type 1, a medium weak class (MW) to type 2, a medium strong class (MS) to type 3, and a strong class (ST) to type 4. It is important to point out that all the 764 roofs analyzed belong to primary structures (i.e., closed constructions that have the functions of housing, services, or commercial use).

Figure 3 illustrates the building roof typology in our survey. Regarding the masonry, 70% of the buildings were regular, 19% irregular, 10% combined and only 0.1% wooden. 46.5% of the buildings were made of a regular plan and simple design, 6.7% regular plan with composite design, and 46.8% with irregular plan and composite design. Regarding roof covering materials: 2.5% metallic, 0.7% fiber cement, zinc or plastic; 50.8% tiles, and 46% concrete. For the roof angle 46.6% was two or more pitches, 46.7% flat, and 6.7% single pitch. In addition, 80% of the surveyed primary buildings had one and 20% two to four storeys. Our findings reveal that 46% of the roofs of our surveyed buildings belong to ST roof class, 34% MS roof class, 17% MW roof class and only 3% WE roof class (Figure 4).

4.2 Occurrence of roof collapse

Overall, 10 roofs out of the 764 surveyed primary buildings were observed to have collapsed due to tephra (Figure 5). One of these roofs was observed to have collapsed during the first field visit and it was later buried by lava (Figure 5H). Out of the remaining nine roofs, seven were observed to have collapsed during the first visit (October 2021, Figures 5A–G) and two were observed to be collapsed after the eruption (Figures 5I, J). The collapsed roofs described in Figure 5 were mainly characterized by metallic, fiber cement/zinc/plastic sheets or tiles. Estimated loads at the time of field observations range between 0.7 and 15 kPa (Figures 6A, B, detailed by zone in Supplementary Figure S3).

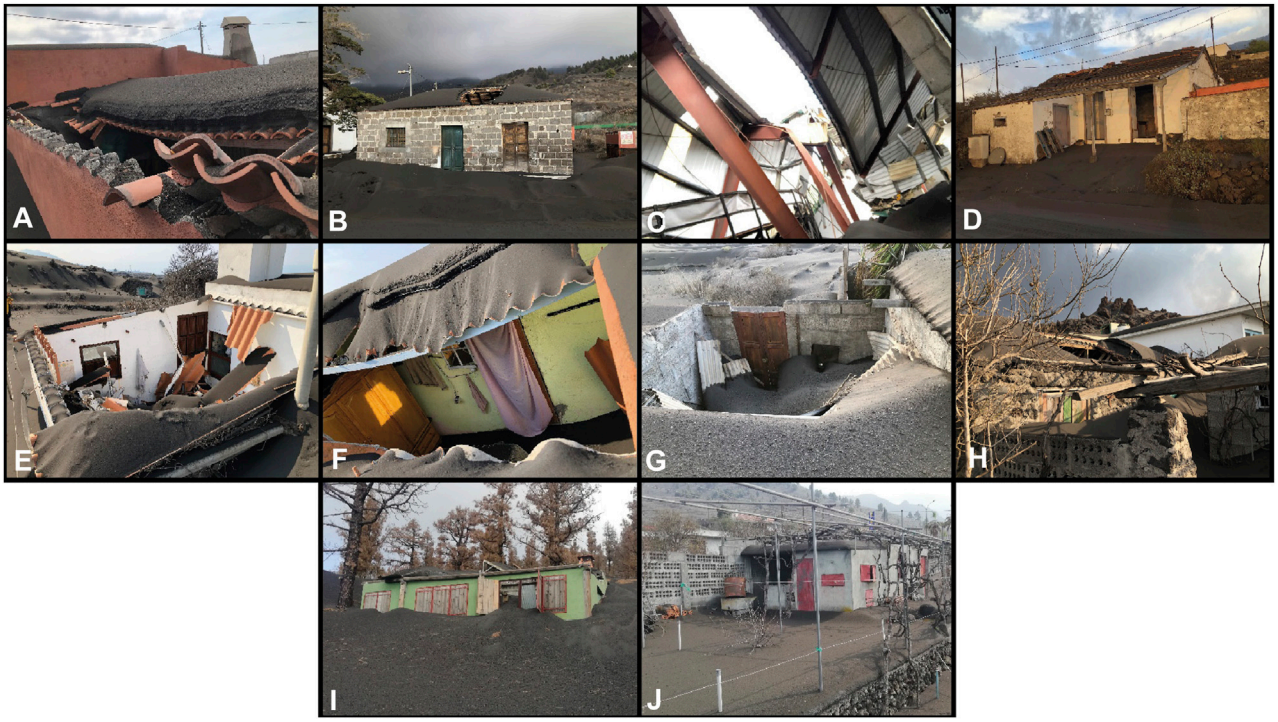

FIGURE 5
Collapsed roofs of primary structures as observed in the field. **(A)** tiled single pitch irregular plan/composite design roof with one storey regular masonry (MS, zone L), **(B)** tiled two or more pitches, regular plan and simple design, with one storey regular masonry (MS, zone B), **(C)** two or more pitches, metallic, regular plan and simple design, with one storey, mixed structure (WE, zone L), **(D)** tiled two or more pitches, regular plan and simple design, with one storey regular masonry (MS, zone H), **(E)** pitched roof of fiber cement/zinc, irregular plan/composite design roof with one storey regular masonry (WE, zone L), **(F)** single pitch of fiber cement/zinc, regular plan and simple design roof with one storey regular masonry (WE, zone L), **(G)** single pitch metallic regular plan and simple design roof with one storey regular masonry (WE, zone L), **(H)** tiled two or more pitches, regular plan and simple design, with one storey irregular masonry (MW, zone L), **(I)** single pitch metallic irregular plan and composite design roof with one storey regular masonry (WE, zone TTLL), **(J)** flat fiber cement/zinc regular plan and simple design roof with one storey regular masonry (WE, zone B).

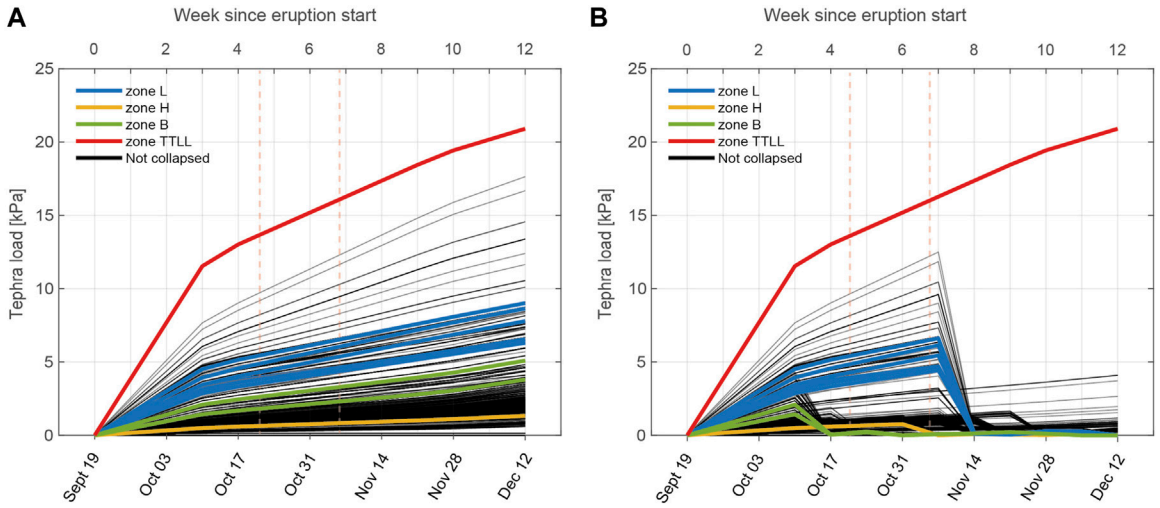

FIGURE 6
Accumulated tephra load (in kPa) over time at the location of the 764 studied buildings (dates on the primary-bottom *x*-axis and weeks since the beginning of the eruption on the secondary-top *x*-axis). All surveyed buildings and zones are considered. Estimated expected loads **(A)** not accounting for clean-up operations; and **(B)** accounting for clean-up operations. Red, blue, green and yellow lines are associated with the buildings with collapsed roofs per UME zone observed in the field. Vertical dashed lines indicate the duration of our first field campaign (21 October—5 November).

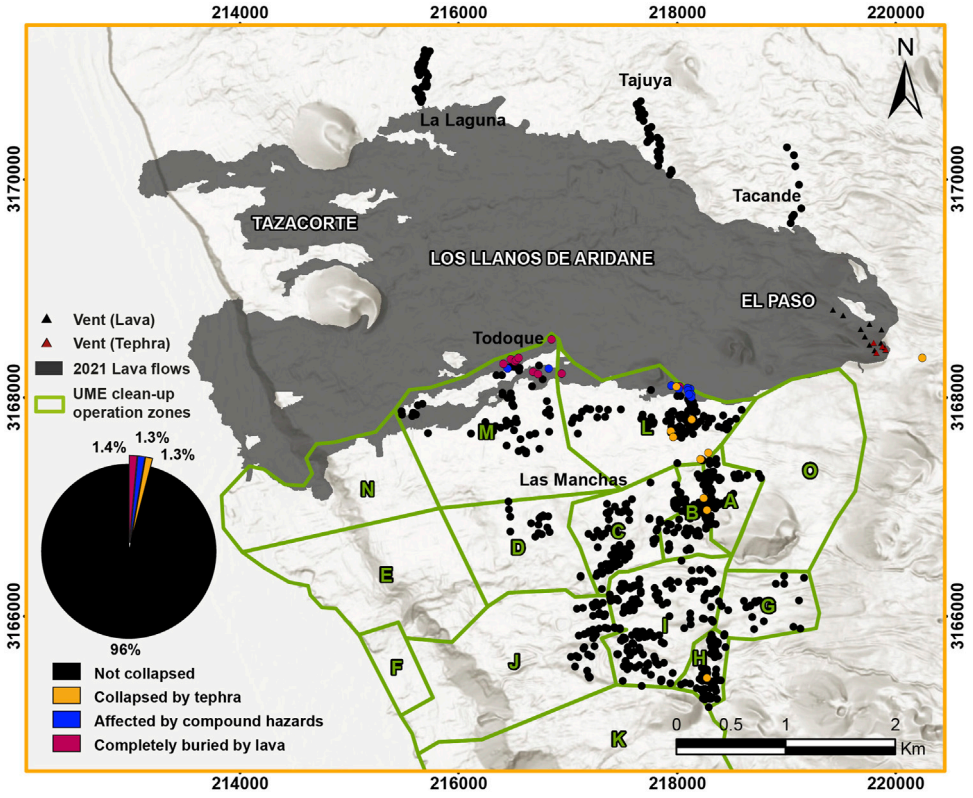

FIGURE 7
Spatial distribution (map) and percentage (pie chart) of the affected roofs from our surveyed buildings associated with the cause of collapse (tephra, lava, or both). The green boundaries show UME clean-up zones.

Furthermore, the spatial distribution of the type of hazard (i.e., lava, tephra, compound lava-tephra hazard) and subsequent impact on roofs (i.e., collapsed by tephra, buried by lava, collapsed by compound lava-tephra hazards, or not affected) is shown in Figure 7. The identified collapsed roofs by tephra are mostly located along or near the municipality boundary that separates Los Llanos de Aridane from El Paso in a N-S direction, within the >20 cm tephra isopach of Bonadonna et al. (2022) with the exception of one located in zone H (Figure 1D); and one is located East of the vent (yellow dots in Figure 1; Figure 7), representing only 1.3% out of the total surveyed buildings (10 buildings: 6 WE, 1 MW and 3 MS). Additionally, 1.3% of the surveyed buildings were affected by both lava and tephra that are not analyzed in this paper (10 buildings of MS vulnerability roof class; blue dots in Figure 7) (Biass et al., 2024). Moreover, at least 1.4% of our surveyed buildings were completely buried by lava (11 buildings: one WE, 1 MW, seven MS and two ST) (red dots in Figure 7).

4.3 Effectiveness of clean-up operations

The effectiveness of clean-up operations on roofs was estimated by comparing roof collapse probabilities with and without accounting for clean-up (Table 3). According to the total load and the vulnerability classes, 20% of the buildings would have equaled or exceeded the 25% probability of roof collapse (n=153) and about 11% of the buildings would have equaled or exceeded the 75% probability of roof collapse (n=86) by the last week of eruption (week 12, Figures 8, 9A). When clean-up operations took place in almost all zones (week 7, see Supplementary Table S1), 7% of buildings would have equaled or surpassed the 75% probability of roof collapse (n=53). By the last week, the percentage of roofs that would have exceeded collapse probabilities of 25% and 75% is reduced to 0.4% (three buildings), and 0.1% (one building), respectively (week 12, Figure 9B).

5 Discussion

5.1 Comparison of observations with models and other eruptions

Collapsed roofs observed during the 2021 Tajogaite eruption provide a comparison with existing fragility curves developed for Europe (Spence et al., 2005). Assuming that no clean-up operations were carried out in zone L prior to our visit in October 2021, the temporal evolution of tephra loads inferred from Figure 6 suggests that roofs in this zone would have collapsed under a load ranging between 4.0 and 6.0 kPa (blue lines in Figure 6). According to the fragility curves of Spence et al. (2005) this range of loads results in collapse probabilities of 100% for all four WE, 92%–100% for the 1 MW roof, and 28%–92% for the single MS building observed in this zone. Conversely, clean-up operations in zones B and H were performed prior to our visit. In the absence of precise constraints on roof collapse dates, we infer maximum loads for the three collapsed roofs in these zones before clean-up (green and yellow lines in

TABLE 3 Comparison of number of roofs that would have potentially collapsed if clean-up operations had not been carried out, number of roofs that would have potentially collapsed even with clean-up operations (after probabilities of roof collapse estimations), and field observations of roofs that actually collapsed. The difference between the uncleaned and cleaned roofs collapsed and the difference between the cleaned and observed roofs collapsed are also included. A percentage of collapse of 25% and 75% is considered (see text for more details). Notice that bold values correspond to the total number of roofs considering all UME clean-up zones.

UME clean-up zones	Roof collapses from total surveyed buildings (n= 764)								
	Not cleaned		Cleaned		Observed	Difference between not-cleaned and cleaned		Difference between cleaned and observed	
	25%	75%	25%	75%		25%	75%	25%	75%
A	38	18	5	0	0	33	18	5	0
B	15	5	1	1	2	14	4	−1	−1
C	7	2	0	0	0	7	2	0	0
D	2	0	0	0	0	2	0	0	0
E	0	0	0	0	0	0	0	0	0
F	0	0	0	0	0	0	0	0	0
G	2	0	0	0	0	2	0	0	0
H	0	0	0	0	1	0	0	−1	−1
I	4	1	0	0	0	4	1	0	0
J	0	0	0	0	0	0	0	0	0
K	0	0	0	0	0	0	0	0	0
L	82	57	57	49	6	25	8	52	44
M	0	0	0	0	0	0	0	0	0
O	0	0	0	0	0	0	0	0	0
TTLL	3	3	3	3	1	0	0	2	2
Total all zones	**153**	**86**	**66**	**53**	**10**	**87**	**33**	**56**	**43**

Figure 6B). In zone B, a load of 3.0 kPa translates to roof collapse probabilities of 98% for the single WE and 2% for the single MS roofs. In zone H, the collapsed MS roof had a virtually null roof collapse probability associated with a load of 0.8 kPa. Although the fragility curves of Spence et al. (2005) performed well in zone L, we attribute the discrepancies observed in zones B and H to four main reasons.

- Firstly, due to access restrictions during our visit, roof properties required to attribute one of the four vulnerability classes were inferred by looking at the building's exterior. In this sense, critical aspects of the roof's structural components (e.g., material and quality of rafters) might have been misinterpreted and a wrong class assigned.
- Secondly, generic vulnerability classes considered in this study represent general roof typologies found across Europe, but they only include those that follow established construction standards. Construction practices such as those found in La Palma (e.g., with extensions of mixed proportions and materials that are added to the more resistant, primary construction) might affect the overall vulnerability of roof.
- Thirdly, the buildings that do not show good agreement with the fragility curves of Spence et al. (2005) (i.e., b, d, and j in Figure 5) possibly correspond to secondary buildings used later for housing, such as garages converted into living spaces (Troll et al., 2023), for which none of the existing fragility curves apply.
- Fourthly, discrepancies might be explained due to clean-up operations, as tephra removal may exacerbate roof damage due to increased static load from people on the roof (Jenkins et al., 2014). Nonetheless, if this was the reason, we should observe more collapses, which is not the case.

Regarding the isolated collapsed roof located in the East of the area, close to the vent (Figure 5I), we cannot constrain the tephra load that collapsed it, since we only observed it after the end of the eruption, and it was never cleaned (red line in Figure 6) (see detailed loads accumulation over time by zone in Supplementary Figure S3).

Comparisons between the taxonomy-type codification of our vulnerability roof classes, Spence et al. (2005); Marti et al. (2008) reveal a good match for WE and ST classes as they have a common roof covering material typology. Our MW class has a good match with Spence et al. (2005) as well but Marti et al. (2008) overlaps with our ST class; and our MS class on the other hand has a mismatch with both, because their MS class overlaps with our ST class as we have considered flat roofs in concrete only for the strongest category (see Table 2).

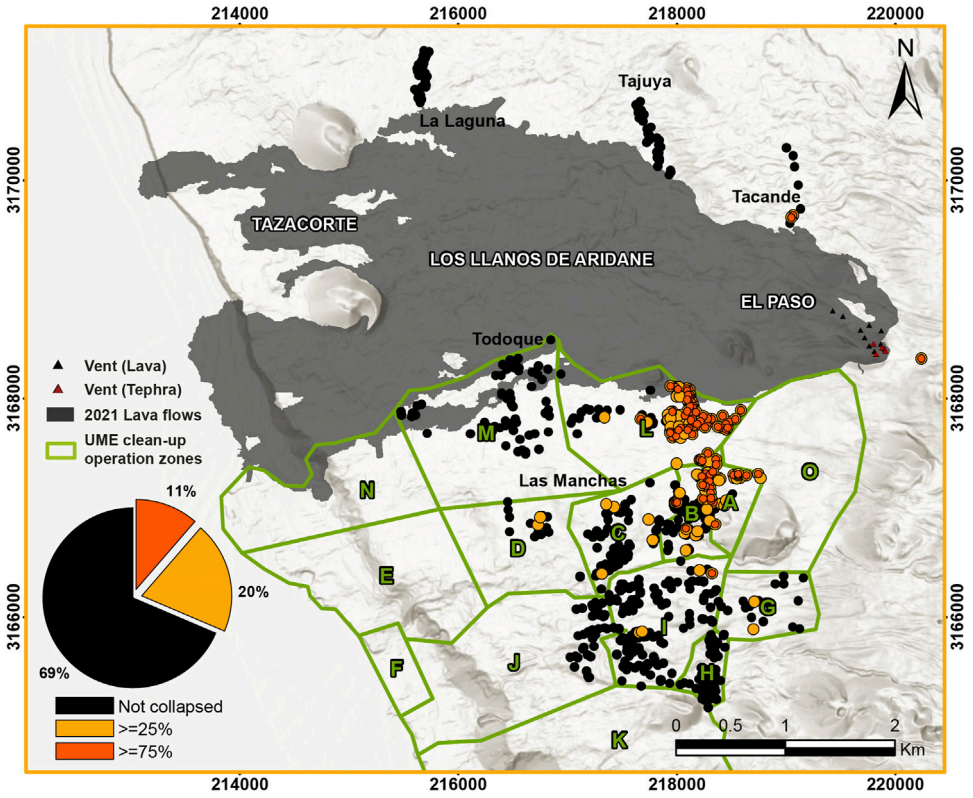

FIGURE 8
Spatial distribution (map) and percentage (pie chart) of potential collapsed roofs from surveyed buildings if clean-up operations had not been carried out associated with two probabilities of collapse (≥25% in yellow and ≥75% in orange). The green boundaries show UME clean-up zones.

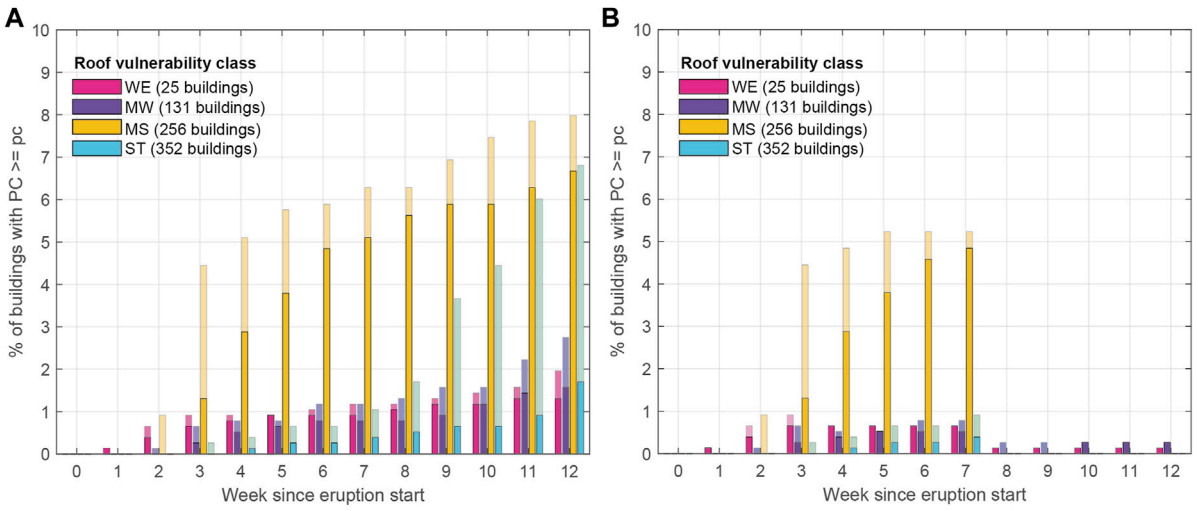

FIGURE 9
Evolution in time (weeks since the beginning of the eruption) of the percentage of the count of buildings that equaled or surpassed a threshold of 25% (light colors) and 75% (dark colors) probability of roof collapse considering two scenarios: **(A)** no clean-up operations carried out; and **(B)** clean-up operations carried out by UME. The surveyed buildings are separated by our vulnerability classes assigned (WE, weak in pink; MW, medium weak in purple; MS, medium strong in yellow; ST, strong in blue).

Using the same fragility curves, observations carried out for other eruptions have recorded roof collapses with similar loads such as the ones found for the Tajogaite eruption (i.e., 0.8–3 kPa) for the same roof class (i.e., WE). For example, during the 2014 Kelud eruption (Indonesia), Williams et al. (2020) remotely studied 1154 buildings that were affected by tephra accumulations of

1–10 cm. Among these only 27 suffered severe roof or building collapse (e.g., clay-tiled roof, supported by timber or bamboo framing), with the heaviest tephra loads being equivalent to 1.4 kPa (Williams et al., 2020). During a post-event damage state framework of the 2015 Calbuco eruption (Chile) for buildings, Hayes et al. (2019) found that total roof collapse occurred with tephra loads of 1.0–3.2 kPa, but also that partial roof collapse may have occurred for tephra loads of 0.2–0.3 kPa. Houses around Calbuco were predominantly timber-framed with metal sheet roofs, and variability in roof pitch, construction quality, and building age (Hayes et al., 2019), which would correspond to a MW roof class, i.e., mean loads of 3.0 kPa. This means these roofs also had little or no probability of collapse following published fragility curves (e.g., Spence et al., 2005; Jenkins et al., 2014). The differences in composition between these eruptions (i.e., Kelud 2014, basaltic andesitic (Cassidy et al., 2019); Calbuco 2015, andesitic (Castruccio et al., 2016); Tajogaite 2021, Tephritic-basanitic (Day et al., 2022b)), have no clear effect in deposit densities, as in agreement with conclusions of Osman et al. (2022) on experiments with different magma compositions and eruption size. This suggests that while roof strengths are predicted reasonably well for previous studies at Vesuvius, Sete Cidades, Soufriere, and Teide (Spence et al., 2005), they may be overestimated for other locations in Europe and construction standards such as some of the buildings we observed in La Palma (i.e., b, d, and j in Figure 5).

The advantage of fragility functions for building roof collapse caused by tephra load accumulation is that they were defined as having a cumulative lognormal distribution with a coefficient of variation of 20%, which allows for uncertainty in the resistance of materials, of structural dimensions, and of load paths (as it may slide off, drift or accumulate on some parts of roof more than others), present to an equal extent in roofs of all types (Spence et al., 2005). Uncertainties of tephra load interpolation reflect uncertainties of the isopach maps, and the bulk density value used. In any case, uncertainties around the evolution of the load might be overshadowed by uncertainties of the roof typology itself.

5.2 Effectiveness and implications of clean-up operations

The emergency management strategy adopted during the 2021 Tajogaite eruption mainly focused on preventing direct human fatalities through evacuations before and during the eruption (Rey et al., 2023). Local authorities had to deal with the unexpected or underestimated effects of the eruption, developing and implementing protocols during the volcanic emergency based on the decisions taken by PEVOLCA (Rey et al., 2023). From eruption onset, an exclusion zone of 2.5 km from the vents and the edge of the lava flow was defined, initially allowing only the firemen to enter. Tephra clean-up operations started only one month later when municipalities and UME were granted access to the restriction zone, adding up on many tasks assumed UME (e.g., hazard monitoring coordination of the air-space, collection of population's belongings during evacuations, psychological support for affected personnel and the organization of community meetings). Even though clean-up operations in La Palma were established after the eruption had already started, they contributed to reduce the impact to the primary residential buildings. Although the availability of pre-established emergency plans can speed up the implementation of such response measure as clean-up operations, authorities might hesitate to begin operations due to uncertainties on the eruption duration and the unwillingness to financially support repeated clean-up operations (e.g., 2002 Etna eruption (Italy), Barnard, (2004)). Weather conditions or large-scale evacuations may also delay clean-up operations to weeks or months after the onset of the eruption [e.g., Jacobacci, 2011 Cordón Caulle eruption (Chile), Wilson et al. (2013); Heimaey, 1973 Eldfell eruption (Iceland), Morgan (2000)].

Here, the effectiveness of clean-up operations of roofs during the 2021 Tajogaite eruption is based on thresholds of roof collapse probabilities of 25% and 75% (Figures 8, 9, and Table 3). These two were arbitrarily chosen to illustrate the variability associated with the fragility curves and are hereafter implied when quantifying the range of collapsed roofs. For collapse thresholds of 25% and 75%, respectively, Figure 8 suggests that 20% and 11% of the surveyed buildings would have suffered roof collapse without clean-up operations, with zone L being the most affected (n = 82 and 57) followed by zone A (n = 38 and 18) and B (n = 15 and 5) (see Table 3, not cleaned). These estimates reflect the spatial distribution of roof collapse observed in the field (i.e., 60% located in zone L, 20% in zone B at the border with zone A, and 10% in zone TTLL), but overestimate the total number of observed collapsed roofs (n = 10, or ~1.3% of all surveyed buildings; Figures 7, 9A). When accounting for clean-up operations, our results suggest that 66 and 53 buildings exceed roof collapse probabilities of 25% and 75%, respectively (Figures 8, 9B, and Table 3, cleaned), which corresponds to a reduction by 57% and 38% of the number of potentially collapsing roofs without clean-up measures. Although these results largely exceed the number of observed collapses (n=10), this theoretical framework supports the importance of clean-up tephra deposits on roofs during long-lasting eruptions as an effective mitigation measure.

The 2021 Tajogaite eruption offers an opportunity to study the widespread impact and crisis management of a long-lasting, hybrid eruption. Starting on September 19, and lasting for about 3 months, the eruption demonstrated how eruptions that are mostly effusive can be associated with widespread tephra deposits (Bonadonna et al., 2022; 2023). However, other critical aspects are also associated with clean-up operations in addition to the risk of roof collapse. First, tephra clean-up operations are challenging, especially due to the uncertainties on the duration, frequency, and spatial distribution of tephra sedimentation and accumulation, and the lack of pre-event planning can increase their costs and reduce its efficiency (Blong, 1984; Wilson et al., 2012; Hayes et al., 2015). Second, clean-up teams are exposed to significant risk of falling from slippery or damaged surfaces or roofs, to remobilized tephra with implications for health, and to back injuries when moving heavy tephra loads (Leonard et al., 2005; Magill et al., 2013; Jenkins et al., 2014; Hayes et al., 2015). Third, clean-up operations result in the accumulation of large volumes of tephra that need to be disposed in dedicated areas, which often cannot be easily identified during the emergency crisis (Magill et al., 2013; Hayes et al., 2015). As a result, the need for clean-up actions must be assessed for each specific volcano and geographic context (Spence et al., 1996). All actions that might improve effectiveness and efficiency of clean-up operations in urban environments rely on pre-event planning (e.g., Hayes, 2014; Hayes et al., 2015; 2017). Actions such as tephra fall hazard assessment (e.g., sources, expected volume and characteristics), identification of land use zoning and roads (e.g., to design routes between tephra pickup points and disposal sites), understanding of societal factors (e.g., economic,

environmental, health and cultural), and development of mutual support arrangements between local or regional operators (e.g., personnel and agency roles) have been identified as crucial aspects to respond to a tephra fall event (Hayes, 2014; Hayes et al., 2015; 2017; 2019; 2021). Moreover, a successful planning for tephra clean-up operations (i.e., cleaning, removal, collection, and disposal) should definitively include an assessment of the likely volume of tephra to be removed, selection of disposal sites (e.g., size, access, ownership, environmental considerations), the possibility of using disposed tephra in the production of construction materials, appropriate methods for clean-up, resource requirements (e.g., street sweepers, fuel and water access), and estimated costs (e.g., Hayes et al., 2015; 2021; Tashima et al., 2023). Recommendation of actions to better prepare, mitigate and reduce ashfall impacts for critical infrastructures are provided by Wilson et al. (2014b) and the USGS (https://volcanoes.usgs.gov/volcanic_ash/), the latter one providing also information specifically for the general public, agencies and scientists.

5.3 Complexity and uncertainty associated with long-lasting, hybrid eruptions

The explosive component of the 2021 Tajogaite eruption was characterized by various eruptive styles (Strombolian, violent Strombolian, lava fountaining, ash-poor gas puffing) occurring either simultaneously or sequentially from different vents with tephra plume heights up to 8.5 km a.s.l. (Bonadonna et al., 2022; 2023; Felpeto et al., 2022). The complex interaction between variable eruptive styles and atmospheric conditions has resulted in large variations in ground accumulation rates in both space and time (Bonadonna et al., 2023). In space, most buildings surveyed in our study area are comprised within the 100 and 5 cm isopach, implying a 20x thickness factor occurring along a maximum downwind distance of 4 km and highlighting the rapid changes in the relevant hazard metrics for roof collapse. In time, tephra accumulation rates could vary between ~2 and >10 kg/m^2/day in zone L between October 26 and November 4 (Bonadonna et al., 2023). This spatio-temporal variability of tephra sedimentation complicates the pre-event impact assessment of eruptions associated with the persistent but unsteady emission of tephra over weeks to months. From a preparedness perspective, these factors increase the uncertainties of hazard assessments related to the identification of the relevant eruption source parameters required for probabilistic modeling [e.g., variations in plume heights, date and duration of the eruption; Biass et al. (2016)]. From a crisis management perspective, the uncertainty on the spatio-temporal variation of accumulation rates complicates the development of emergency plans. Usually, that local temporary interruptions of tephra sedimentation (e.g., changes on the eruptive styles and/or wind directions) offer opportunistic windows for mitigation actions such as clean-up operations that should be recognised in emergency response but are difficult to predict.

5.4 Limitations

The information within this paper is of both qualitative and quantitative nature, derived from satellite images, field observations, data provided by stakeholders, and probabilistic estimates of roof collapse. This approach facilitated the data collection for the study of the evolution of tephra sedimentation and the associated physical impacts on roofs, which represents one of the major challenges of post-eruption impact assessments. There are some limitations which are also important to highlight:

- For simplicity and homogeneity of data, we focused our study only on roof collapses of primary buildings due to tephra load in the SW area of the island. However, we also observed that secondary and annex structures (e.g., garages, warehouses, storages, outdoor kitchens) suffered the most severe damage and collapses because they were inherently weaker and never cleaned.
- Having studied a fraction of the buildings of some of the impacted areas, our datasets on roof collapse is incomplete. For example, zone O (Figure 1) could have impacted many buildings, but it was impossible to survey because, by the time of our fieldtrip, they were buried by tephra and consequently no longer visible, with no access, or getting very close to the vent, therefore not safe.
- We only considered the tephra load and one specific damage state for buildings (i.e., roof collapse). Nonetheless, there are many additional primary damaging characteristics of tephra (e.g., loading, thickness, dispersal, grainsize, surface chemistry and abrasiveness) and impact metrics that can be used to evaluate the volcanic impact intensity for a particular element at risk such as roofs and entire buildings (e.g., damage percentage, loss of function, damage index, damage state, among others).
- Tephra was dispersed over the whole island and might have impacted buildings in other ways other than roof collapse. For example, erosion and remobilization by wind or water might have limited the access to buildings, and infiltration through openings might have caused blockages (e.g., air and water filters). Additionally, other elements at risk such as critical infrastructure (e.g., transportation, power, water storage and treatment tanks, telecommunication), emergency facilities (e.g., police stations, fire stations), critical facilities (e.g., schools), and economic activities (e.g., agriculture, livestock, tourism) were also disrupted in addition to residential buildings (Dominguez et al., 2022; Rey et al., 2023).
- Our clean-up information might not be complete since other organizations, in addition to the UME, were involved in the tephra cleaning, as well as building owners when authorized. We also assumed that for each cleaning date in a certain zone, the whole tephra load was removed.

6 Conclusion

The combination of field analysis of both roof vulnerability and damage state during and after the 2021 Tajogaite eruption, high-resolution satellite imagery, information from local stakeholders on the timing of clean-up operations, fragility curves and reconstruction of the evolution of the tephra blanket provided key insights into risk management of long-lasting, hybrid eruptions. Organized tephra clean-up operations during long-lasting eruptions are shown to be an effective measure to mitigate the risk of roof collapse.

Our analysis based on the fragility curves of Spence et al. (2005) suggests that if no clean-up measure had been taken at least 11% of the surveyed buildings would have exceeded a 75% probability of roof

collapse (i.e., 86 roofs), while only 7% would have exceeded the same probability when clean-up operations are considered (i.e., 53 roofs). In reality, only 10 buildings have been observed to collapse. Based on this comparison, we conclude that although our estimate is associated with an inherent variability coming from the use of generic fragility curves, well-designed clean-up operations plans represent an effective way to mitigate impacts on the built environment and should be included within volcanic risk reduction plans.

Finally, the combined occurrence of hazards from both effusive and explosive styles during the 2021 Tajogaite eruption highlights the necessity of developing multi-hazard impact framework that not only consider the superimposition of disconnected hazardous phenomena but account for their potential to cause compound impacts (Fink and Aijbade, 2022). Regarding the physical vulnerability of buildings, new multi-hazard taxonomies such as Global Exposure Database for all (GED4All, Silva et al., 2018) have been proposed to collect exposure data in a structured way and support multi-hazard risk assessment (Murnane et al., 2019). Homogenization of pre-event exposure and vulnerability investigations as well as post-event impact assessments should be systematically carried out in the future, for all geophysical hazards.

Data availability statement

The raw data supporting the conclusion of this article will be made available by the authors, without undue reservation.

Author contributions

M-PR-H: Conceptualization, Data curation, Formal Analysis, Investigation, Methodology, Visualization, Writing–original draft, Writing–review and editing. SB: Conceptualization, Data curation, Formal Analysis, Investigation, Methodology, Supervision, Validation, Visualization, Writing–original draft, Writing–review and editing. LD: Formal Analysis, Investigation, Methodology, Supervision, Validation, Writing–review and editing, Conceptualization. LSDM: Investigation, Methodology, Writing–review and editing. CF: Formal Analysis, Investigation, Methodology, Supervision, Validation, Writing–review and editing. CB: Conceptualization, Formal Analysis, Funding acquisition, Resources, Supervision, Validation, Visualization, Writing–review and editing. NP: Writing–review and editing.

Funding

The author(s) declare financial support was received for the research, authorship, and/or publication of this article. This study is funded by the SNSF project #200021_188757.

Acknowledgments

We thank the Instituto Volcanológico de Canarias (INVOLCAN) for their logistic support that was essential for the development of this work. Sincere thanks to comandante Manuel Burgos and teniente coronel Jose Alberto Gallego Lopez from UME for providing key information for our analysis. The authors are also grateful to Julio Rodriguez Diaz and Pedro Garcia Salguero who provided us the photo in Figure 2A and allowed us to sample and photograph on their property. We thank the population of the affected areas for their availability and for their inspiring resilience. CS, JMDD and the editors are thanked for their thoughtful comments.

Conflict of interest

The authors declare that the research was conducted in the absence of any commercial or financial relationships that could be construed as a potential conflict of interest.

Publisher's note

All claims expressed in this article are solely those of the authors and do not necessarily represent those of their affiliated organizations, or those of the publisher, the editors and the reviewers. Any product that may be evaluated in this article, or claim that may be made by its manufacturer, is not guaranteed or endorsed by the publisher.

Supplementary material

The Supplementary Material for this article can be found online at: https://www.frontiersin.org/articles/10.3389/feart.2023.1303330/full#supplementary-material

References

Albertos, V. T., Recio, G., Alonso, M., Amonte, C., Rodríguez, F., Rodríguez, C., et al. (2022). "Sulphur dioxide (SO2) emissions by means of miniDOAS measurements during the 2021 eruption of Cumbre Vieja volcano, La Palma, Canary Islands," in *EGU general assembly 2022* (Vienna, Austria), 23–27. May 2022, EGU22-5603. doi:10.5194/egusphere-egu22-5603

Ancochea, E., Hernán, F., Cendrero, A., Cantagrel, J. M., Fúster, J., Ibarrola, E., et al. (1994). Constructive and destructive episodes in the building of a young oceanic island, La Palma, canary islands, and genesis of the Caldera de Taburiente. *J. Volcanol. Geotherm. Res.* 60 (3-4), 243–262. doi:10.1016/0377-0273(94)90054-X

Andreastuti, S., Paripurno, E., Gunawan, H., Budianto, A., Syahbana, D., and Pallister, J. (2019). Character of community response to volcanic crises at Sinabung and Kelud volcanoes. *J. Volcanol. Geotherm. Res.* 382, 298–310. doi:10.1016/j.jvolgeores.2017.01.022

Baggio, C., Bernardini, A., Colozza, R., Corazza, L., Bella, M. D., Pasquale, G. D. I., et al. (2007). *Field Manual for post-earthquake damage and safety assessment and short term countermeasures (AeDES)*. Luxemburg: European Commission—Joint Research Centre—Institute for the Protection and Security of the Citizen. EUR, 22868.

Barnard, S. T. (2004). Results of a reconnaissance trip to Mt. Etna, Italy. *Bull. New Zeal. Soc. Earthq. Eng.* 37, 47–61. doi:10.5459/bnzsee.37.2.47-61

Biass, S., Bonadonna, C., di Traglia, F., Pistolesi, M., Rosi, M., and Lestuzzi, P. (2016). Probabilistic evaluation of the physical impact of future tephra fallout events for the Island of Vulcano, Italy. *Bull. Volcanol.* 78, 37–22. doi:10.1007/s00445-016-1028-1

Biass, S., Reyes-Hardy, M-P., Gregg, C., Di Maio, L. S., Dominguez, L., Frischknecht, C., et al. (2024). The spatiotemporal evolution of compound impacts from lava flow and tephra fallout on buildings: lessons from the 2021 Tajogaite eruption (La Palma, Spain). *Bull. Volcanol.* doi:10.1007/s00445-023-01700-w

Blake, D. M., Wilson, G., Stewart, C., Craig, H., Hayes, J. L., Jenkins, S. F., et al. (2015). Impacts of the 2014 eruption of Kelud volcano, Indonesia, on infrastructure, utilities, agriculture and health.

Blong, R. (2003). Building damage in rabaul, Papua New Guinea, 1994. *Bull. Volcanol.* 65, 43–54. doi:10.1007/s00445-002-0238-x

Blong, R. J. (1984). *Volcanic hazards: a sourcebook on the effects of eruptions*. London, UK: Acad. Press.

Bonadonna, C., Biass, S., Menoni, S., and Gregg, C. E. (2021). "Assessment of risk associated with tephra-related hazards," in *Forecasting and planning for volcanic hazards, risks, and disasters* (Elsevier), 329–378. doi:10.1016/B978-0-12-818082-2.00008-1

Bonadonna, C., Pistolesi, M., Biass, S., Voloschina, M., Romero, J., Coppola, D., et al. (2022). Physical characterization of long-lasting hybrid eruptions: the 2021 Cumbre Vieja eruption of La Palma (canary islands, Spain). *J. Geophys. Res. Solid Earth*. doi:10.1029/2022JB025302

Bonadonna, C., Pistolesi, M., Dominguez, L., Freret-lorgeril, V., Rossi, E., Fries, A., et al. (2023). Tephra sedimentation and grainsize associated with pulsatory activity: the 2021 tajogaite eruption of Cumbre Vieja (La Palma, canary islands, Spain). *Front. Earth Sci.* 11. doi:10.3389/feart.2023.1166073

Carracedo, J. C., Badiola, E. R., Guillou, H., De La Nuez, J., and Pérez Torrado, F. J. (2001). Geología y vulcanología de La Palma y El Hierro, Canarias occidentales. *Estud. Geol.* 57, 175–273. doi:10.3989/egeol.01575-6134

Carracedo, J. C., Day, S. J., Guillou, H., and Gravestock, P. (1999a). Later stages of volcanic evolution of La Palma, Canary Islands: rift evolution, giant landslides, and the genesis of the Caldera de Taburiente. *Geol. Soc. Am. Bull.* 111, 755–768. doi:10.1130/0016-7606(1999)111<0755:LSOVEO>2.3.CO;2

Carracedo, J. C., Day, S. J., Guillou, H., and Pérez Torrado, F. J. (1999b). Giant quaternary landslides in the evolution of La Palma and El Hierro, canary islands. *J. Volcanol. Geotherm. Res.* 94, 169–190. doi:10.1016/S0377-0273(99)00102-X

Carracedo, J. C., and Troll, V. (2016). *The geology of the canary islands*. Elsevier.

Carracedo, J. C., Troll, V. R., Day, J. M., Geiger, H., Aulinas, M., Soler, V., et al. (2022). The 2021 eruption of the Cumbre Vieja volcanic ridge on La Palma, canary islands. *Geol. Today* 38 (3), 94–107. doi:10.1111/gto.12388

Cassidy, M., Ebmeier, S. K., Helo, C., Watt, S. F. L., Caudron, C., Odell, A., et al. (2019). Explosive eruptions with little warning: experimental petrology and volcano monitoring observations from the 2014 eruption of Kelud, Indonesia. *Geochem. Geophys. Geosystems* 20 (8), 4218–4247. doi:10.1029/2018GC008161

Castruccio, A., Clavero, J., Segura, A., Samaniego, P., Roche, O., Le Pennec, J.-L., et al. (2016). Eruptive parameters and dynamics of the April 2015 sub-Plinian eruptions of Calbuco volcano (southern Chile). *Bull. Volcanol.* 78, 62–19. doi:10.1007/s00445-016-1058-8

Civico, R., Ricci, T., Scarlato, P., Taddeucci, J., Andronico, D., Del Bello, E., et al. (2022). High-resolution digital surface model of the 2021 eruption deposit of Cumbre Vieja volcano, La Palma, Spain. *Sci. Data* 9 (1), 435. doi:10.1038/s41597-022-01551-8

Comisión mixta para la reconstrucción and, recuperación y apoyo a la isla de LA. PALMA (2022). Informe sobre las actuaciones y medidas emprendidas tras la erupción del volcán de Cumbre Vieja (La Palma), seis meses después del inicio de la emergencia.

Day, J. M. D., Geiger, H., Troll, V. R., Perez-Torrado, F. J., Aulinas, M., Gisbert, G., et al. (2022a). Bouncing spallation bombs during the 2021 La Palma eruption, canary islands, Spain. *Earth Sci. Syst. Soc.* 2, 1–9. doi:10.3389/esss.2022.10063

Day, J. M. D., Troll, V. R., Aulinas, M., Deegan, F. M., Geiger, H., Carracedo, J. C., et al. (2022b). Mantle source characteristics and magmatic processes during the 2021 La Palma eruption. *Earth Planet. Sci. Lett.* 597, 117793. doi:10.1016/j.epsl.2022.117793

De Bélizal, É., Lavigne, F., Gaillard, J. C., Grancher, D., Pratomo, I., and Komorowski, J.-C. (2012). The 2007 eruption of Kelut volcano (East Java, Indonesia): phenomenology, crisis management and social response. *Geomorphology* 136 (1), 165–175. doi:10.1016/j.geomorph.2011.06.015

Dominguez, L., Bonadonna, C., Frischknecht, C., Menoni, S., and Garcia, A. (2021). Integrative post-event impact assessment framework for volcanic eruptions: a disaster forensic investigation of the 2011–2012 eruption of the Cordón Caulle volcano (Chile). *Front. Earth Sci.* 9, 645945. doi:10.3389/feart.2021.645945

Dominguez, L., Frischknecht, C., Reyes-Hardy, M.-P., Di Maio, L., Bonadonna, C., and Pérez, N. (2022). "Oral presentation: the 2021-Cumbre Vieja eruption (La Palma, Spain): multi-hazard scenarios and cascading impacts," in 11th Conference Cities on Volcanoes (COV11) June 12-17, 2022, Heraklion, Crete (Greece).

Douglas, J. (2007). Physical vulnerability modelling in natural hazard risk assessment. *Nat. Hazards Earth Syst. Sci.* 7 (2), 283–288. doi:10.5194/nhess-7-283-2007

EN 1998-1 (2004). Eurocode 8: design of structures for earthquake resistance – Part 1: general rules, seismic actions and rules for buildings. [Authority Eur. Union Per Regul. 305/2011, Dir. 98/34/EC, Dir. 2004/18/EC]. Available at: https://www.phd.eng.br/wp-content/uploads/2015/02/en.1998.1.2004.pdf.

Felpeto, A., Molina-Arias, A. J., Quirós, F., Pereda, J., García-Cañada, L., and Díaz-Suárez, E. A. (2022). Measuring the height of the eruptive column during the 2021 eruption of Cumbre Vieja (La Palma island, canary islands). *EGU General Assem. Conf. Abstr*. doi:10.5194/egusphere-egu22-9419

Fink, J., and Ajibade, I. (2022). Future impacts of climate-induced compound disasters on volcano hazard assessment. *Bull. Volcanol.* 84, 42. doi:10.1007/s00445-022-01542-y

Gommers, R., Virtanen, P., Burovski, E., Weckesser, W., Oliphant, T. E., Haberland, M., et al. (2022). scipy/scipy: SciPy 1.9.0rc2. doi:10.5281/ZENODO.6796035

G. Grünthal (1998). *European Macroseismic Scale 1998 (EMS-98). Conseil de l'Europe*. (Luxembourg: Cahiers du Centre Européen de Géodynamique et de Séismologie), 15. doi:10.2312/EMS-98.full.en

GVP (2023). Global volcanism Program, 2023. Holocene volcanoes of the world (v. 5.1.1; 17 aug 2023). Distributed by smithsonian institution, compiled by venzke, E. Available at:. doi:10.5479/si.GVP.VOTW5-2023.5.1

Hayer, C., Barrancos, J., Burton, M., Rodríguez, F., Esse, B., Hernández, P., et al. (2022). From up above to down below: comparison of satellite- and ground-based observations of SO 2 emissions from the 2021 eruption of Cumbre Vieja, La Palma. *EGU General Assem. Conf. Abstr*. doi:10.5194/egusphere-egu22-12201

Hayes, J. (2014). *Tephra clean-up in Auckland City, New Zealand: quantitative impact assessment and response planning*. doi:10.26021/5782

Hayes, J., Wilson, T. M., Deligne, N. I., Cole, J., and Hughes, M. (2017). A model to assess tephra clean-up requirements in urban environments. *J. Appl. Volcanol.* 6, 1–23. doi:10.1186/s13617-016-0052-3

Hayes, J. L., Wilson, T. M., Brown, C., Deligne, N. I., Leonard, G. S., and Cole, J. (2021). Assessing urban disaster waste management requirements after volcanic eruptions. *Int. J. Disaster Risk Reduct.* 52, 101935. doi:10.1016/j.ijdrr.2020.101935

Hayes, J. L., Wilson, T. M., and Magill, C. (2015). Tephra fall clean-up in urban environments. *J. Volcanol. Geotherm. Res.* 304, 359–377. doi:10.1016/j.jvolgeores.2015.09.014

Hayes, J. L., Wilson, T. M., Stewart, C., Villarosa, G., Salgado, P., Beigt, D., et al. (2019). Tephra clean-up after the 2015 eruption of Calbuco volcano, Chile: a quantitative geospatial assessment in four communities. *J. Appl. Volcanol.* 8, 7–23. doi:10.1186/s13617-019-0087-3

Hernández-Pacheco, A. (1990). *La erupción del Tahuya en 1585 y el origen de los Roques de Jedey, La Palma, Canarias*. Tenerife, Spain: Secr. Publicaciones, Universidad de La Laguna.

Hernandez-Pacheco, A., and Valls, M. C. (1982). The historic eruptions of La Palma island (Canaries). Arquipélago. *Série Ciências Nat.* 3, 83–94. Available at: http://hdl.handle.net/10400.3/4915.

Hoyer, S., Roos, M., Joseph, H., Magin, J., Cherian, D., Fitzgerald, C., et al. (2022). Xarray (v0.21.0). *Zenodo*. doi:10.5281/zenodo.5914998

Jenkins, S. F., Day, S. J., Faria, B. V. E., and Fonseca, J. F. B. D. (2017). Damage from lava flows: insights from the 2014–2015 eruption of Fogo, Cape Verde. *J. Appl. Volcanol.* 6 (1), 6–17. doi:10.1186/s13617-017-0057-6

Jenkins, S. F., Spence, R. J. S., Fonseca, J. F. B. D., Solidum, R. U., and Wilson, T. M. (2014). Volcanic risk assessment: quantifying physical vulnerability in the built environment. *J. Volcanol. Geotherm. Res.* 276, 105–120. doi:10.1016/j.jvolgeores.2014.03.002

Jenkins, S. F., Wilson, T. M., Magill, C., Miller, V., Stewart, C., Blong, R., et al. (2015). "Volcanic ash fall hazard and risk," in *Global volcanic hazards and risk* (Cambridge University Press), 173–222. doi:10.1017/CBO9781316276273.005

Klügel, A., Schmincke, H.-U., White, J. D., and Hoernle, K. (1999). Chronology and volcanology of the 1949 multi-vent rift-zone eruption on La Palma (Canary Islands). *J. Volcanol. Geotherm. Res.* 94 (1-4), 267–282. doi:10.1016/S0377-0273(99)00107-9

Leonard, G. S., Johnston, D. M., Williams, S., Cole, J. W., Finnis, K., and Barnard, S. T. (2005). Impacts and management of recent volcanic eruptions in Ecuador: lessons for New Zealand. *GNS Sci. Rep.* 20, 35.

Lev, E., Birnbaum, J., Hernandez, P., Barrancos, J., Tramontano, S., Connor, L., et al. (2022). Lava flow dynamics during the 2021 Cumbre Vieja eruption, La. *EGU General Assem. Conf. Abstr*. doi:10.5194/egusphere-egu22-10531

Lindell, M. K., and Perry, R. W. (1993). "Risk area residents' changing perceptions of volcano hazard at Mt. St.Helens," in *Prediction and perception of natural hazards*. Editors F. Siccardi, J. Nigg, and J. Nemec (Amsterdam: Kluwer Academic Publishers).

Longpré, M.-A. (2021). Reactivation of Cumbre Vieja volcano. *Science* 374, 1197–1198. doi:10.1126/science.abm9423

López, R. P., Sánchez-jiménez, E. U. N., Mediato, J. F., López-gutiérrez, J., Mateo, R. M., Martí-, J., et al. (2021). La erupción volcánica de Cumbre Vieja en La Palma. *Consor Seguros Rev. Digit.* 15, 1–16. Available at: https://www.consorsegurosdigital.com/es/numero-16/portada/la-erupcion-volcanica-de-cumbre-vieja-en-la-palma-2021.

Magill, C., Wilson, T., and Okada, T. (2013). Observations of tephra fall impacts from the 2011 Shinmoedake eruption, Japan. *Earth, Planets Sp.* 65, 677–698. doi:10.5047/eps.2013.05.010

Marrero, J. M., García, A., Llinares, A., De la Cruz-Reyna, S., Ramos, S., and Ortiz, R. (2013). Virtual tools for volcanic crisis management, and evacuation decision support: applications to El Chichón volcano (Chiapas, México). *Nat. Hazards* 68, 955–980. doi:10.1007/s11069-013-0672-4

Marti, J., Spence, R., Calogero, E., Ordoñez, A., Felpeto, A., and Baxter, P. (2008). Estimating building exposure and impact to volcanic hazards in Icod de los Vinos,

Tenerife (Canary Islands). *J. Volcanol. Geotherm. Res.* 178 (3), 553–561. doi:10.1016/j.jvolgeores.2008.07.010

Martín-Lorenzo, A., Andronico, D., Rodríguez, F., Coldwell, B., Pankhurst, M., Taddeucci, J., et al. (2022). Preliminary results from textural studies on tephra deposits erupted during the 2021 eruption at Cumbre Vieja volcano. *EGU General Assem. Conf. Abstr.* doi:10.5194/egusphere-egu22-9986

Mei, E. T. W., Lavigne, F., Picquout, A., de Bélizal, E., Brunstein, D., Grancher, D., et al. (2013). Lessons learned from the 2010 evacuations at Merapi volcano. *J. Volcanol. Geotherm. Res.* 261, 348–365. doi:10.1016/j.jvolgeores.2013.03.010

Ministerio de Hacienda y Función Pública (2014). Modelo de datos de cartografia vectorial (Formato Shapefile). 23. Available at: http://www.geogra.uah.es/gisweb/practica-vectorial/Formato_Shapefile.htm.

Morgan, A. V. (2000). The Eldfell eruption Heimaey, Iceland: a 25-year retrospective. *Geosci. Can.* 27 (1), 11–18. Accessed https://journals.lib.unb.ca/index.php/GC/article/view/4030%0A%0A.

Murnane, R., Fraser, S., Giovando, C., Phillips, E., Loughlin, S., Duncan, M., et al. (2019). Extensible data schemas for multiple hazards, exposure and vulnerability data. *Contrib. Pap. GAR*, 1–20.

Osman, S., Thomas, M., Crummy, J., and Carver, S. (2022). Investigation of geomechanical properties of tephra relevant to roof loading for application in vulnerability analyses. *J. Appl. Volcanol.* 11 (1), 9–17. doi:10.1186/s13617-022-00121-2

PEVOLCA (2023). Certificado PEVOLCA 07/07/2023. Available at: https://riesgovolcanico-lapalma.hub.arcgis.com/documents/693c976dfb9645fc88cd6f94a5ebd194/explore.

Pioli, L., Azzopardi, B. J., and Cashman, K. V. (2009). Controls on the explosivity of scoria cone eruptions: magma segregation at conduit junctions. *J. Volcanol. Geotherm. Res.* 186 (3-4), 407–415. doi:10.1016/j.jvolgeores.2009.07.014

Praegel, N. O. (1986). The petrology and geochemistry of volcan teneguía, La Palma, canary islands: tables and Figures. *Inst. Pet. Københavns Univ*.

Rey, T., Leone, F., Candela, T., Defossez, S., Parat, F., Gherardi, M., et al. (2023). L'éruption du Tajogaite (Cumbre Vieja) à La Palma, Canaries: de l'éruption volcanique à la crise territoriale. *EchoGéo En. ligne]*. doi:10.4000/echogeo.24450

Romero, J. E., Burton, M., Cáceres, F., Taddeucci, J., Civico, R., Ricci, T., et al. (2022). The initial phase of the 2021 Cumbre Vieja ridge eruption (Canary Islands): products and dynamics controlling edifice growth and collapse. *J. Volcanol. Geotherm. Res.* 431, 107642. doi:10.1016/j.jvolgeores.2022.107642

Romero, R., and del Carmen, M. (1990). Las manifestaciones volcánicas históricas del Archipiélago Canario. Available at: http://riull.ull.es/xmlui/handle/915/10113.

Romero Ortiz, J. (1951). La erupcion del Nambroque en la Isla de La Palma. *Bol. Inst. Geol. Min. Esp.*, 1–165. doi:10.1007/BF02598189

San Miguel de la Cámara, M., Fúster Casas, J. M., and Martel, Y. (1952). Las erupciones y materiales arrojados por ellas en la Isla de La Palma — junio-Julio de 1949. *Bull. Volcanol.* 12, 145–163. doi:10.1007/BF02596019

Santiago, M. (1960). Los volcanes de La Palma (islas Canarias). *Datos Histórico-descriptivos. El Mus. Canar.* 21, 281–346.

Silva, V., Yepes-Estrada, C., Dabbeek, J., Martins, L., and Brzev, S. (2018). GED4ALL - global exposure Database for multi- hazard risk analysis – multi-hazard exposure taxonomy. *mGEM Tech. Rep.* 2018-01, *GEM Found. Pavia, Italy*. Available at: https://www.gfdrr.org/sites/default/files/publication/Exposuredataschema_finalreport.pdf.

Spence, R., Pomonis, A., Baxter, P. J., Coburn, A. W., White, M., and Dayrir, M. (1996). "Building damage caused by the mount pinatubo eruption of june 15, 1991," in *Fire and mud: eruptions and lahars of mount pinatubo, Philippines and lahars of mount pinatubo, Philippines*. Editors C. G. Newhall and R. S. Punongbayan, 1055–1062.

Spence, R. J. S., Kelman, I., Baxter, P. J., Zuccaro, G., and Petrazzuoli, S. (2005). Residential building and occupant vulnerability to tephra fall. *Nat. Hazards Earth Syst. Sci.* 5 (4), 477–494. doi:10.5194/nhess-5-477-2005

Taddeucci, J., Scarlato, P., Andronico, D., Ricci, T., Civico, R., Del Bello, E., et al. (2023). The explosive activity of the 2021 tajogaite eruption (La Palma, canary islands, Spain). *Geochem. Geophys. Geosystems* 24 (6), 1–21. doi:10.1029/2023GC010946

Tashima, M. M., Soriano, L., Borrachero, M. V., Monzó, J., and Payá, J. (2023). Towards the valorization of Cumbre Vieja volcanic ash – production of alternative cements. *Constr. Build. Mat.* 370, 130635. doi:10.1016/j.conbuildmat.2023.130635

Tomsen, E., Lindsay, J. M., Gahegan, M., Wilson, T. M., and Blake, D. M. (2014). Evacuation planning in the Auckland Volcanic Field, New Zealand: a spatio-temporal approach for emergency management and transportation network decisions. *J. Appl. Volcanol.* 3 (1), 6–22. doi:10.1186/2191-5040-3-6

Troll, V. R., Aulinas, M., Carracedo, J. C., Geiger, H., Soler, V., Deegan, F. M., et al. (2023). The 2021 La Palma eruption; social dilemmas resulting from living close to an active volcano. *Preprint*. doi:10.31223/X5QX1M

UNISDR (2009). *Terminology on disaster risk reduction*. Geneva: United Nations Publ, 35.

Wadsworth, F. B., Llewellin, E. W., Castro, J. M., Tuffen, H., Schipper, C. I., Gardner, J. E., et al. (2022). A reappraisal of explosive-effusive silicic eruption dynamics: syn-eruptive assembly of lava from the products of cryptic fragmentation. *J. Volcanol. Geotherm.* 432, 107672. doi:10.1016/j.jvolgeores.2022.107672

Walter, T. R., and Troll, V. R. (2003). Experiments on rift zone evolution in unstable volcanic edifices. *J. Volcanol. Geotherm. Res.* 127 (1-2), 107–120. doi:10.1016/S0377-0273(03)00181-1

White, J. D. L., and Schmincke, H.-U. (1999). Phreatomagmatic eruptive and depositional processes during the 1949 eruption on La Palma (Canary Islands). *J. Volcanol. Geotherm. Res.* 94 (1-4), 283–304. doi:10.1016/S0377-0273(99)00108-0

Williams, G. T., Jenkins, S. F., Biass, S., Wibowo, H. E., and Harijoko, A. (2020). Remotely assessing tephra fall building damage and vulnerability: Kelud Volcano, Indonesia. *J. Appl. Volcanol.* 9, 10–18. doi:10.1186/s13617-020-00100-5

Wilson, G., Wilson, T. M., Deligne, N. I., Blake, D. M., and Cole, J. W. (2017). Framework for developing volcanic fragility and vulnerability functions for critical infrastructure. *J. Appl. Volcanol.* 6, 14–24. doi:10.1186/s13617-017-0065-6

Wilson, G., Wilson, T. M., Deligne, N. I., and Cole, J. W. (2014a). Volcanic hazard impacts to critical infrastructure: a review. *J. Volcanol. Geotherm. Res.* 286, 148–182. doi:10.1016/j.jvolgeores.2014.08.030

Wilson, T., Kaye, G., Stewart, C., and Cole, J. (2007). Impacts of the 2006 eruption of Merapi volcano, Indonesia, on agriculture and infrastructure. *GNS Sci. Rep*. 2007/07. Available at: http://ir.canterbury.ac.nz/handle/10092/760.

Wilson, T., Stewart, C., Bickerton, H., Baxter, P., Outes, V., Villarosa, G., et al. (2013). Impacts of the June 2011 Puyehue-Cordón Caulle volcanic complex eruption on urban infrastructure, agriculture and public health. *GNS Sci. Rep.*, 2012–2020.

Wilson, T. M., Cole, J. W., Stewart, C., Cronin, S. J., and Johnston, D. M. (2011). Ash storms: impacts of wind-remobilised volcanic ash on rural communities and agriculture following the 1991 Hudson eruption, southern Patagonia, Chile. *Bull. Volcanol.* 73, 223–239. doi:10.1007/s00445-010-0396-1

Wilson, T. M., Stewart, C., Sword-Daniels, V., Leonard, G. S., Johnston, D. M., Cole, J. W., et al. (2012). Volcanic ash impacts on critical infrastructure. *Phys. Chem. Earth, Parts A/B/C* 45, 5–23. doi:10.1016/j.pce.2011.06.006

Wilson, T. M., Stewart, C., Wardman, J. B., Wilson, G., Johnston, D. M., Hill, D., et al. (2014b). Volcanic ashfall preparedness poster series: a collaborative process for reducing the vulnerability of critical infrastructure. *J. Appl. Volcanol.* 3, 10–25. doi:10.1186/s13617-014-0010-x

Zuccaro, G., Cacace, F., Spence, R. J. S., and Baxter, P. J. (2008). Impact of explosive eruption scenarios at Vesuvius. *J. Volcanol. Geotherm. Res.* 178 (3), 416–453. doi:10.1016/j.jvolgeores.2008.01.005